Nanoparticle-Based Platform for Activatable Fluorescence Imaging and Photothermal Ablation of Endometriosis

Abraham S. Moses,

College of Pharmacy, Oregon State University, 2730 SW Moody Avenue, Portland, OR 97201, USA

Olena R. Taratula,

College of Pharmacy, Oregon State University, 2730 SW Moody Avenue, Portland, OR 97201, USA

Hyelim Lee,

College of Pharmacy, Oregon State University, 2730 SW Moody Avenue, Portland, OR 97201, USA

Fangzhou Luo,

Division of Reproductive and Developmental Sciences, Oregon National Primate Research Center, Oregon Health & Science University, 505 NW 185th Avenue, Beaverton, OR 97006, USA

Tanner Grenz,

Division of Reproductive and Developmental Sciences, Oregon National Primate Research Center, Oregon Health & Science University, 505 NW 185th Avenue, Beaverton, OR 97006, USA

Tetiana Korzun,

College of Pharmacy, Oregon State University, 2730 SW Moody Avenue, Portland, OR 97201, USA

Anna St Lorenz,

College of Pharmacy, Oregon State University, 2730 SW Moody Avenue, Portland, OR 97201, USA

Fahad Y. Sabei,

College of Pharmacy, Oregon State University, 2730 SW Moody Avenue, Portland, OR 97201, USA

Shay Bracha,

Carlson College of Veterinary Medicine, Oregon State University, 700 SW 30th Street, Corvallis, OR 97331, USA

Adam W. G. Alani,

oleh.taratula@oregonstate.edu, slaydeno@ohsu.edu.

Conflict of Interest
The authors declare no conflict of interest.

College of Pharmacy, Oregon State University, 2730 SW Moody Avenue, Portland, OR 97201, USA

Ov D. Slayden,

Division of Reproductive and Developmental Sciences, Oregon National Primate Research Center, Oregon Health & Science University, 505 NW 185th Avenue, Beaverton, OR 97006, USA

Oleh Taratula

College of Pharmacy, Oregon State University, 2730 SW Moody Avenue, Portland, OR 97201, USA

Abstract

Endometriosis is a painful disorder where endometrium-like tissue forms lesions outside of the uterine cavity. Intraoperative identification and removal of these lesions are difficult. This study presents a nanoplatform that concurrently delineates and ablates endometriosis tissues using real-time near-infrared (NIR) fluorescence and photothermal therapy (PTT). The nanoplatform consists of a dye, silicon naphthalocyanine (SiNc), capable of both NIR fluorescence imaging and PTT, and a polymeric nanoparticle as a SiNc carrier to endometriosis tissue following systemic administration. To achieve high contrast during fluorescence imaging of endometriotic lesions, nanoparticles are constructed to be non-fluorescent prior to internalization by endometriosis cells. In vitro studies confirm that these nanoparticles activate the fluorescence signal following internalization in macaque endometrial stromal cells and ablate them by increasing cellular temperature to 53 °C upon interaction with NIR light. To demonstrate in vivo efficiency of the nanoparticles, biopsies of endometrium and endometriosis from rhesus macaques are transplanted into immunodeficient mice. Imaging with the intraoperative Fluobeam 800 system reveals that 24 h following intravenous injection, nanoparticles efficiently accumulate in, and demarcate, endometriotic grafts with fluorescence. Finally, the nanoparticles increase the temperature of endometriotic grafts up to 47 °C upon exposure to NIR light, completely eradicating them after a single treatment.

Keywords

endometriosis; fluorescence imaging; nanoparticles; photothermal therapy

1. Introduction

Endometriosis is a non-cancerous gynecological disorder defined by the presence of endometrium-like cells outside of the uterus.[1-4] The ectopic endometrium creates lesions that cause pelvic pain and infertility.[5-7] It affects ≈10% of childbearing-age women and 20–50% of women with subfertility. Despite recent advances in medical therapy to treat endometriosis-related pelvic pain, there remains no medical cure for this disease. Surgical removal of the lesions is often considered a treatment option for women wishing to improve fertility.[8,9] Unfortunately, recurrence of the disease after surgery can exceed 50%, with 27% of patients requiring three or more surgeries.[10,11] Ongoing retrograde menstruation with renewed seeding could contribute to disease recurrence. However, a key factor leading to recurrence is the presence of minute endometriotic residues after surgery.[12] Therefore,

there is a need for novel strategies that can improve real-time visualization and intraoperative treatment of endometriotic lesions in women. Achieving both goals can further eliminate occult disease sites that are difficult to distinguish from non-endometriotic tissue in real-time or that are challenging to resect without damaging healthy organs.

Clinical trials and preclinical studies verified that fluorescence image guidance has significant potential to aid surgeons in the identification of malignant lesions in real-time. [13-16] A human trial proved that under fluorescence guidance, the number of ovarian cancer tumors resected by surgeons increased by 5.3-fold, compared with traditional surgery.[13] Previous reports also suggested that intraoperative adjuvant therapies delivered immediately after tumor resection can maximize the efficiency of surgery by destroying unresected residual cancer lesions.[16,17] One promising intraoperative treatment modality is photothermal therapy (PTT),[18-25] which is highly efficient and has minimal side effects because it selectively destroys cancer cells with heat generated by non-toxic photoactive agents after their activation with targeted light. The fluorescence signal emitted by these agents can also enable monitoring of their accumulation within cancer tissue and allows for precise focusing of light onto the tumors to activate heat generation.[26-29] Taking these facts into consideration, it is reasonable to hypothesize that fluorescence-guided surgery and intraoperative photothermal therapy can substantially reduce the post-surgical recurrence of endometriosis. In order to determine the potential of this treatment in preclinical studies and utilize it in clinic, simple and highly efficient imaging and phototherapeutic agents with high translational potential are required. To avoid multiple administrations of separate imaging and therapeutic agents, it is essential to use a single platform that possesses both fluorescence imaging and PTT functions. Importantly, as this platform will be used only during surgical treatment, its imaging and therapeutic efficiency must be very effective with a single dose. Finally, this platform must be biocompatible, efficiently accumulate in endometriosis lesions after systemic administration, provide a high endometriosis-to-normal tissue contrast ratio, and generate high temperatures in endometriotic lesions upon exposure to targeted light.

Herein, we report a biocompatible nanoparticle-based platform that efficiently delineates endometriotic lesions engrafted in mice with real-time near-infrared (NIR) fluorescence following a single intravenous administration. To provide high endometriosis-to-normal tissue contrast, the nanoplatform is constructed to be non-fluorescent in systemic circulation and to emit NIR fluorescence only after accumulation in the endometriosis cells. Furthermore, the same nanoparticles efficiently increase the temperature inside of endometriotic grafts upon exposure to NIR light and completely eradicate them with a single dose of phototherapy.

2. Results and Discussion

2.1. Preparation of Nanoplatform for Fluorescence Imaging and Photothermal Therapy

A highly photostable dye, silicon naphthalocyanine (SiNc, Figure 1),[23,30] was selected as a building block for the construction of a single-agent based nanoplatform capable of NIR fluorescence imaging and photothermal therapy (PTT).

Previous reports reveal that SiNc exhibits strong absorption of NIR light and can generate both high NIR fluorescence and heat upon exposure to NIR light of relatively low power (>0.3 W cm^{-2}).[23,30] These photophysical properties are highly desirable for sensitive fluorescence imaging and photothermal eradication of endometriotic lesions, because biological tissues and body fluids exhibit reduced autofluorescence, and are relatively transparent to the excitation light, in the NIR optical window (700–900 nm).[31-33]

To overcome challenges associated with poor solubility and aggregation of SiNc in aqueous environments, the solvent evaporation approach was employed to encapsulate SiNc molecules within the hydrophobic core of (methoxy poly(ethylene glycol)-*b*-poly(*ε*-caprolactone)) (PEG-PCL)-based polymeric nanoparticles.[23,34] The amphiphilic PEG-PCL molecules, composed of hydrophobic 10 kDa PCL and hydrophilic 5 kDa PEG blocks, self-assemble in aqueous solution upon evaporation of the organic solvent, tetrahydrofuran, to form nanoparticles with a hydrophilic PEG outer shell and hydrophobic PCL core (Figure 1). Dynamic light scattering and zeta potential measurements revealed that the constructed SiNc-loaded polymeric nanoparticles (SiNc-NP) have a hydrodynamic size of ≈40 nm (Figure 2A) with monodispersed size distribution (polydispersity index = 0.048) and slightly negative surface charge (−2.8 mV). The representative cryo-transmission electron microscope (TEM) image confirms that monodispersed nanoparticles with a spherical shape were prepared (Figure 2B).

To achieve high contrast during the fluorescence imaging of endometriotic lesions, SiNc-NP were constructed to be non-fluorescent prior to internalization into endometriosis cells. SiNc-NP with "always on" fluorescence were reformulated to produce non-fluorescent SiNc-NP ("activatable" SiNc-NP) by increasing the amount of SiNc molecules in the hydrophobic core of PEG-PCL nanoparticles from 0.5% to 6% of SiNc per 1 mg of PEG-PCL (Figures 1 and 2C). Our previous studies revealed that dense packing of SiNc molecules within the hydrophobic core of nanoparticles results in self-quenching of their fluorescence.[34] The solution study in PBS buffer at pH 7.4 demonstrated the negligible release of SiNc dye from SiNc-NP at 37 °C (Figure S1A, Supporting Information).

2.2. In Vitro Evaluation of Fluorescence Imaging and PTT Mediated by SiNc-NP

Imaging and photothermal properties of the constructed SiNc-NP were evaluated on rhesus macaque endometriotic stromal cells collected from a monkey with spontaneous endometriosis. By using SiNc-NP with "always on" fluorescence, we confirmed that the developed nanoparticles can be rapidly and efficiently internalized by endometriotic stromal cells. Figure 3 (top panel) demonstrates that a strong NIR fluorescence signal was detected inside endometriotic cells in as little as 1 h following incubation with these nanoparticles.

Fluorescence spectra of the internalized nanoparticles into endometriotic cells were also recorded with fluorescence spectrophotometer (Figure S1B, Supporting Information). In contrast, initially non-fluorescent SiNc-NP ("activatable" SiNc-NP) of the same size, shape, and surface charge as SiNc-NP with "always on" fluorescence, emitted a dim fluorescence signal inside cells only at 4 h post-incubation, which reached its maximum intensity at ≈24 h.

This fluorescence microscopy study suggests that the initially non-fluorescent "activatable" nanoparticles emit fluorescence signal only after internalization by endometriotic stromal cells. The obtained results are in good agreement with our previous report indicating that the self-assembled structure of PEG-PCL polymeric nanoparticles can be compromised in the intracellular environment of cancer cells.[34] Consequently, dense packing of SiNc molecules inside the hydrophobic cores of PEG-PCL nanoparticles is disrupted, resulting in NIR fluorescence activation (Figure 1).

To validate the efficacy of SiNc-NP-mediated photothermal therapy for endometriosis treatment, endometriotic stromal cells were incubated with a non-toxic concentration of "activatable" SiNc-NP (30 μg mL^{-1}) for 48 h and the loosely-pelleted cells were then illuminated with 780 nm NIR light (0.9 W cm^{-2}) for 15 min. During the NIR light exposure, the temperature inside of cell pellets rapidly increased from ≈37 °C to ≈53 °C, which caused more than 95% endometriotic cell death (Figure 4, bar 6). In contrast, NIR light exposure of non-treated cells and cells treated with empty PEG-PCL nanoparticles (without SiNc) resulted in negligible temperature changes (<0.3 °C) and, consequently, viability of endometriotic cells was not compromised (Figure 4, bars 2 and 4).

2.3. Development and Characterization of a Mouse Model for Endometriosis

To develop an animal model for endometriosis, biopsies of endometrium and endometriosis were collected from three adult rhesus macaques with advanced (Stage 4) endometriosis and transplanted subcutaneously into severe combined immunodeficient (SCID) female mice (four grafts per mouse). We previously verified that macaque endometrium can be engrafted into these mice resulting in endometriotic lesions similar to those in macaque.[35] At the time of graft placement, animals were treated with implants (Innovative Research of America) releasing estradiol (E$_2$) and progesterone (P$_4$) to create artificial primate-length hormonal cycles in the mice. This permits experiments that recapitulate the primate menstrual cycle in the mice. All mice engrafted with macaque endometriotic grafts developed subcutaneous lesions. After two artificial cycles, the average graft "take" rate was 77.5 + 5.9%. Of the mice examined, 100% of the grafts displayed endometriotic glands and stroma (Figure 5) and were immunocytochemically positive for estrogen receptor 1 (ESR1, Figure 5A) and progesterone receptor (PGR, Figure 5B).

The presence of these receptors demonstrates the hormonal responsiveness of the grafts, which is identical to endometriosis in macaques.[36] As expected, there were abundant proliferating cells as detected by KI-67 staining (Figure 5C), indicating that the lesions were growing in response to estrogen stimulation. Staining for Factor 8 revealed that the grafts were well vascularized (Figure 5D). Due to the hormone responsiveness of these grafts and the observation that the grafts are highly vascularized, the developed animal model was used for assessment of imaging and PTT properties of the "activatable" SiNc-NP in vivo.

2.4. In Vivo Evaluation of SiNc-NP for Imaging of Endometriotic Lesions

Potential acute toxicity of "activatable" SiNc-NP on various organs was evaluated by measuring the concentrations of surrogate biomarkers in the blood for kidney function (blood urea nitrogen and Creatinine), liver function (alkaline phosphatase and alanine

aminotransferase), muscle and heart function (creatine kinase) (Table S1, Supporting Information), and the serum levels of blood electrolytes (Table S2, Supporting Information) and proteins (Table S3, Supporting Information) as an indicator of major organ toxicity. The measured values in non-treated mice (control) and mice injected with the SiNc-NP via tail vein were not statistically different, suggesting that the developed nanoparticles do not exhibit any acute toxicity.

To evaluate the ability of the constructed nanoparticles to delineate endometriotic lesions with NIR fluorescence signal following systemic administration, mice with subcutaneous macaque endometriotic grafts were injected via tail vein with "activatable" SiNc-NP (3 mg kg^{-1} of SiNc). Whole-body photographic and fluorescence images of mice acquired with both the FDA-approved intraoperative imaging system Fluobeam 800 and Pearl Impulse Small Animal Imaging System revealed that "activatable" SiNc-NP accumulate in endometriotic lesions, activate their NIR fluorescence 24 h following a single injection, and precisely demarcate endometriotic lesions (Figure 6A,B). Ex vivo fluorescence images of the resected organs and endometriotic lesions further confirmed that the NIR fluorescence signal was predominantly localized in endometriotic lesions, providing high endometriosis-to-normal tissue contrast during SiNc-NP-mediated fluorescence imaging (Figure 6C).

The obtained results are in agreement with our previous studies demonstrating that SiNc-NP efficiently accumulates in ovarian cancer xenografts following systemic administration.[34] It is believed that nanoparticles in systemic circulation leak preferentially into tumor tissue through permeable tumor vessels and are then retained in the tumor bed due to reduced lymphatic drainage.[37] The similar biodistribution profiles of SiNc-NP in mice with cancer and mice with endometriotic grafts following intravenous injection could be explained by the fact that both cancer and endometriosis are angiogenesis-dependent diseases and the nanoparticles can accumulate in tumors and endometriotic lesions by extravasation through permeable blood vessels.[38,39] Angiogenesis represents a key factor in the growth and development of endometriotic lesions, and growing evidence in the primary literature supports a role for vascular endothelial growth factor in both the regulation of neovascularization and the increased permeability of endometriotic vascularity.[40] Immunostaining of the sectioned tissues with both Factor 8 (Figure 5D) and CD31 (Figure 6D,E) antibodies revealed the extensive vascular development in the endometriotic grafts used in our experiments that parallels angiogenesis in lesions in both macaques and women. Histological assessment further confirmed penetration and accumulation of SiNc-NP into endometriotic lesions following extravasation from the blood vessels (Figure 6D,E). As such, our results and previous reports[39] suggest that long-circulating nanoparticles can efficiently accumulate in endometriotic lesions after systemic administration due to their extravasation through leaky vasculature, and that nanoparticle-based systems such as the developed SiNc-NP offer novel and less invasive opportunities for treatment and imaging of endometriosis.

The reason that the NIR fluorescence signal was predominantly detected in endometriotic lesions after systemic injection of "activatable" SiNc-NP (Figure 6C) is related to the fact that the activation of SiNc fluorescence primarily occurred in the intracellular environment (Figure 3). Because the biodistribution studies with "always on" SiNc-NP revealed that, in

addition to endometriotic lesions, our nanoparticles can accumulate in other organs (e.g., kidneys, Figure S2, Supporting Information), it is reasonable to assume that "activatable" SiNc-NP might also activate their fluorescence following internalization into healthy cells (e.g., kidneys). In vitro studies, however, verified that the internalization efficiency of the developed SiNc-NP by kidney cells (Figure S3, Supporting Information) is minimal in comparison to endometriotic cells (Figure 3). These differences could be explained by the fact that our PEG-PCL-based nanoparticles enter the cells by endocytosis[41] and endometriotic cells differentially express endocytotic pathways compared to non-diseased cells.[42] Aberrations in endocytotic processes lead to differential uptake of nanoparticles inside endometriotic cells when compared to normal cells.

2.5. In Vivo Assessment of SiNc-NP-Mediated Photothermal Therapy for Eradication of Endometriotic Lesions

To further evaluate the therapeutic potential of photothermal therapy for treatment of endometriotic lesions, mice bearing multiple endometriosis grafts (four grafts per mouse) were injected via tail vein with the "activatable" SiNc-NP (3 mg SiNc kg^{-1}) and 2 grafts in every mouse were exposed to NIR light (780 nm, 0.9 W cm^{-2}) for 15 min at 24 h post-injection. The other 2 grafts without NIR light treatment were used as controls to evaluate the effect of SiNc-NP alone on the growth of endometriotic lesions. Direct temperature measurements with a fiber optic probe demonstrated that SiNc-NP rapidly increased the temperature inside of endometriotic grafts up to 47 °C upon exposure to NIR light (Figure 7A) and treated grafts were completely eradicated within 4 days following a single treatment, with no recurrence in the 7-week study (Figure 7B).

In contrast, endometriotic grafts were not affected by SiNc-NP alone (without NIR exposure) or NIR laser alone, and their growth rate was similar to non-treated lesions (Figure 7B).

Our studies validated that the NIR light alone (780 nm, 0.9 W cm^{-2}) increased the temperature of endometriotic grafts by less than 1 °C (Figure 7A). Therefore, the employed light is safe for photothermal therapy, because it is incapable of non-specific tissue heating during treatment. Finally, the treated mice showed no signs of toxicity (e.g., behavior, appearance, etc.) and their body weights gradually increased during the 7-week study (Figure 7C), suggesting that SiNc-NP-mediated PTT is safe without any adverse effects.

Histological analysis revealed that loss of graft glands and stroma was accompanied by a loss of ESR1 and PGR staining in PTT-treated grafts (Figure 8B,D,F,H) when compared to non-treated ones (Figure 8A,C,E,G). Reduction in steroid receptor expression in the PTT-treated endometriotic tissue indicates a loss of both hormonal responsiveness and potential for growth under estrogen.

3. Conclusion

We constructed "activatable" SiNc-NP that efficiently delineate endometriotic lesions with NIR fluorescence signal and rapidly eliminate them by PTT. We validated that, following intravenous administration, the developed nanoparticles efficiently reach vasculature of

primate endometriotic grafts and further extravasate from the blood vessels into the endometriotic tissue. NIR fluorescence signal generated by the delivered nanoparticles is retained predominantly in endometriotic lesions, providing high endometriosis-to-normal tissue contrast during fluorescence imaging. Upon exposure to targeted NIR light, the same nanoparticles also efficiently generate heat within endometriotic lesions, destroying them. Loss of ESR1 and PGR in the residual graft tissue further suggests that the remaining endometriotic tissue will no longer respond to estrogen stimulation. We conclude that the obtained results justify further evaluation of the developed nanoplatform for fluorescence-guided surgery and intraoperative PTT in macaques with spontaneous endometriotic lesions. Validation of this treatment approach in macaques that develop endometriosis anatomically similar to that found in humans is essential before advancing the therapeutic modality to human clinical trials.

4.   Experimental Section

Materials:

SiNc (silicon 2,3-naphthalocyanine bis (trihexylsilyloxide)) and PEG–PCL (methoxy poly(ethylene glycol)-*b*-poly(*ε*-caprolactone), MW: PEG(5k)-PCL(10k)) were purchased from Alfa Chemistry (Ronkonkoma NY), and Advanced Polymer Materials Inc. (Montreal, Canada), respectively. Other chemicals and supplies were obtained from VWR International, LLC (Radnor, PA).

Synthesis and Characterization of SiNc-NP:

SiNc-NP were prepared using the solvent evaporation method as previously reported.[23,34] Briefly, SiNc and PEG-PCL were dissolved in tetrahydrofuran (THF), combined in specific ratios to produce "always on" (0.5% SiNc per 1 mg PEG-PCL, formulation with fluorescence properties) and "activatable" SiNc-NP (6% SiNc per 1 mg PEG-PCL, formulation with quenched fluorescence) while stirring, and then mixed with 0.9% sodium chloride solution for 5 min. Then, THF was removed using a rotovap (Heidolph, Schwabach, Germany). Next, the prepared samples were filtered and further characterized by following previously reported procedures.[23,34,43-48] Briefly, size, polydispersity index (determined through dynamic light scattering), and zeta potential of nanoparticles were measured using a Zetasizer (Malvern Panalytical, Malvern, UK).[44,46] Absorption and fluorescence spectra were recorded on a UV-VIS-NIR spectrophotometer (Shimadzu, Kyoto, Japan) and fluorescence spectrophotometer (Agilent Technologies, Santa Clara, California), respectively.[48] The presence ("always on") or absence ("activatable") of SiNc-NP's fluorescence signal was confirmed using a Pearl Impulse fluorescence imaging system (LI-COR, Lincoln, NE).[34] The shape of SiNc-NP was visualized on a Tecnai Spirit TEM (Tecnai, Hillsboro, OR).[43]

Primary Cell Cultures:

Cell culture methods have been modified from those reported by Haining et al.[49] as follows. Endometriosis tissues collected from two rhesus macaques at necropsy were digested with collagenase and DNase (Worthington, Lakewood, NJ, USA) at 37 °C in F10 media (Sigma Aldrich, St. Louis, MO, USA) to dissociate the cells. The cells were passed

through a 70 μm nylon cell strainer, centrifuged, and suspended in Modified Eagle's Medium supplemented with 10% Fetal Bovine Serum plus antibiotic and antimycotic. Cells were seeded into the wells of sterile 6-well plates at a density of 2.0×10^5 cells per well. After cell attachment, wells were washed with medium and when the cells reached 90% confluence, they were passaged for transfer to T-25 culture flasks and medium that was changed every 4 days.

In Vitro Evaluation of SiNc-NP Toxicity:

Primary macaque endometriosis cells were seeded in a 96-well plate at a density of 1.0×10^4 cells per well, and incubated with 0, 10, 20, or 30 μg mL^{-1} of SiNc (in SiNc-NP) for 48 h. Cell viability was determined using Calcein AM assay (Corning Inc., Corning, NY) as previously reported.[44]

Nanoparticle Cellular Internalization:

Primary macaque endometriosis cells were seeded into a 12-well plate at a density of $\approx 1.0 \times 10^5$ cells per well, and incubated with both "always on" and "activatable" SiNc-NP at a concentration of 30 μg SiNc mL^{-1} for 1, 2, 4, and 24 h. Cells were then rinsed with Dulbecco's Phosphate Buffered Saline (DPBS) and fixed using 4% paraformaldehyde in DPBS. Cell nuclei were stained using NucBlue Fixed Cell ReadyProbes Reagent (ThermoFisher Scientific, Waltham, Massachusetts), and fluorescence images were acquired using a fluorescence microscope (Keyence, Osaka, Japan) with DAPI (ex./em. 360/460nm) and Cy7 (ex./em. 710/810 nm) fluorescence filters.

In Vitro Phototherapy Treatment:

Monolayers of primary macaque endometriosis cells were incubated with "activatable" SiNc-NP at a concentration of 30 μg SiNc mL^{-1} for 48 h. Cells were then rinsed, trypsinized, and collected. Cells were loosely pelleted, submerged in 50 μL of DPBS and exposed to NIR (780 nm, 0.9 W cm^{-2}) laser at a distance of ≈ 1 cm for 15 min.[23] Temperatures were recorded immediately following laser treatment using a fiber optic thermal probe (Neoptix, Québec, Canada).[23] Cells were then resuspended in complete growth media and seeded in a 96-well plate at a density of 1.0×10^4 cells per well. Following recovery (≈ 18 h), Calcein AM assay was performed to evaluate post-treatment cell viability.[23] Pellets of non-treated cells, cells incubated with the same concentration of SiNc-NP under dark conditions, and non-treated cells exposed to a 780 nm laser diode for 15 min were used as controls.

Engraftment of Endometriosis in Immunodeficient Mice:

Animal studies were reviewed and approved by the Oregon Health & Science University (OHSU) and Oregon National Primate Research Center (ONPRC) Institutional Animal Care and Use Committees. Adult rhesus macaques ($n = 3$) with advanced (Stage 4) endometriosis were identified in the research colony at ONPRC. Macaque endometrium and endometriotic lesions were collected at necropsy from adult cycling rhesus macaques (*Macaca mulata*) and transported to the laboratory in sterile Belzer Cold Storage Solution (Fisher Scientific) at 4 °C. Explants (16–21 mm^3) were prepared by first slicing tissues and cutting 4–5 mm^2

biopsies 1 mm thick. Random samples of all biopsies were immediately frozen in Tissue Tek optimal cutting temperature (OCT) compound (Miles Laboratories Elkhart IL), cryosectioned, and assessed for the presence of endometrium-like glands and stroma. The remaining biopsies were transplanted subcutaneously into immunodeficient SCID mice.

Female (21 days old) ICR SCID mice were purchased from Taconic Biosciences (Germantown NY) and housed under barrier husbandry conditions in the OHSU West Campus Small Laboratory Animal Unit (SLAU). Procedures for engraftment of human endometriosis into immunodeficient mice had been published previously.[50] In this study, procedures were carried out in biosafety cabinets housed in the SLAU. The mice were anesthetized with 1.5–4% isoflurane during grafting and steroid implant procedures. Immediately prior to engraftment, the mice received implants releasing estradiol (E_2; 0.5 mg, 90-day release) and progesterone (P_4; 5 mg 14-day release; Innovative Research of America). Monkey endometriotic tissue was placed into subcutaneous pockets under the dorsal and flank skin (four to six grafts per mouse). Buprenorphine SR (0.3 mg kg^{-1}) was administered subcutaneously to the mice at the completion of grafting procedures. The release of P_4 from the implants declined after 14 days, and the P_4 implants were replaced on cycle day 30 to create an artificial primate-length hormonal cycle. After completing two artificial cycles the mice ($n = 21$) were transferred to the laboratory where they were used for evaluation of imaging and PTT properties of the developed "activatable" SiNc-NP. At the time of imaging and PTT studies, all mice were under E_2 treatment alone.

Grafts were excised from additional mice ($n = 14$) and either fixed in 4% paraformaldehyde and embedded in paraffin, or frozen in OCT compound for cryosectioning. All of these grafts were examined histologically for the presence of endometriosis. Immunohistochemistry (IHC) for ESR1, PGR, cell proliferation (KI-67) and von Willebrand factor (Factor 8) was performed on tissue sections after microwave stabilization as described previously.[50] Slides bearing the cryosections were microwave stabilized and fixed in 2% paraformaldehyde in PBS (pH 7.3; Sigma) for 10 min at room temperature (≈23 °C). Endogenous peroxidase activity was inhibited by incubating the slides in a solution of glucose oxidase (1 U mL^{-1}), sodium azide (1 mM L^{-1}), and glucose (10 mM L^{-1}) in PBS for 45 min. Primary antibodies for IHC included: anti ESR1 (1D-5; ThermoFisher, Rockford IL), anti-PGR (hPRa2; ThermoFisher, Rockford IL) anti-KI-67 antigen (Clone EP5; BioGenex), Factor 8 (F8-5.5.72; ThermoFisher). Color was developed with an avidin-biotin peroxidase kit (Vector Labs) with 0.025% diaminobenzidine to visualize antibody-antigen complexes, which were stabilized with 0.026% osmium tetroxide. Slides were lightly counterstained with hematoxylin. Photomicrographs were captured with a Leica DMC 6200 camera through a Zeiss Axioimager.

In Vivo Imaging Studies:

Five mice bearing subcutaneous endometriotic xenografts were systemically administered with "activatable" SiNc-NP (3 mg SiNc kg^{-1}) via lateral tail-vein injection. Whole-body photographic and fluorescence images were acquired 24 h post-injection with a Pearl Impulse fluorescence imaging system (LI-COR, Lincoln, NE) and Fluobeam 800 (Fluoptics, France). Afterward, mice were euthanized and their organs and endometriotic grafts resected

and imaged with a Pearl Impulse fluorescence imaging system. Finally, endometriotic tissues were embedded in OCT compound (Sakura Finetek, Torrance, California), and cryosectioned using a CM 1860 Cryostat (Leica, Wetzlar, Germany). Histological sections were then stained for vascular endothelia using CD-31 antibody (Abcam, Cambridge, UK) as a marker for angiogenesis,[51] and imaged using a fluorescence microscope (Keyence, Osaka, Japan) with GFP (ex./em. 470/525 nm) and Cy7 (ex./em. 710/810 nm) fluorescence filters for visualization of blood vessels and SiNc, respectively.

In Vivo Photothermal Therapy Studies:

Ten mice bearing multiple endometriotic grafts (four grafts per mouse) were divided into two groups (five mice per group). Mice in the first and second groups were intravenously injected with "activatable" SiNc-NP (3 mg kg^{-1}) and saline, respectively. Mice were anesthetized 24 h post-injection and two grafts in each mouse were exposed to a 780 nm laser (0.9 W cm^{-2}) for 15 min. Length and width of endometriotic grafts were measured using calipers during 45 days following treatment and used to calculate grafts volume according to the Equation (1):

$$V = W(2) \times L / 2 \tag{1}$$

where V, W, and L are volume, width, and length of lesions, respectively. Mice were then euthanized and dissected to inspect endometriotic lesion sites. The collected grafts were examined histologically for the presence of endometriosis as described earlier.

To evaluate temperature changes inside of endometriotic grafts during PTT or exposure to a 780 nm laser (0.9 W cm^{-2}) alone, two separate groups of mice (three mice per group) were intravenously injected with "activatable" SiNc-NP (3 mg kg^{-1}) and saline, respectively. Prior to laser exposure, a fiber optic thermal probe (Neoptix Inc., QC, Canada) was inserted into grafts through an 18-gauge needle. Temperature was recorded during laser exposure using Neolink software (Neolink Technologies, Kerala, India).

Statistical Analysis:

Data were analyzed using descriptive statistics and presented as mean value ± standard deviation (SD) from 3–5 separate measurements. Comparisons among groups were executed using independent samples Student's t-tests. Differences between groups were considered statistically significant at $p < 0.05$.

Supplementary Material

Refer to Web version on PubMed Central for supplementary material.

Acknowledgements

References

[1]. Vercellini P, Vigano P, Somigliana E, Fedele L, Nat. Rev. Endocrinol 2014, 10, 261. [PubMed: 24366116]

[2]. Brosens IA, Am. J. Obstet. Gynecol 1997, 176, 263. [PubMed: 9065165]

[3]. Burney RO, Giudice LC, Fertil. Steril 2012, 98, 511. [PubMed: 22819144]

[4]. Martin DC, Ling FW, Clin. Obstet. Gynecol 1999, 42, 664. [PubMed: 10451777]

[5]. Giudice LC, Kao LC, Lancet 2004, 364, 1789. [PubMed: 15541453]

[6]. Ferrero S, Remorgida V, Venturini PL, Clin. Evid 2010, 2010.

[7]. Ozkan S, Murk W, Arici A, Ann. N. Y. Acad. Sci 2008, 1127, 92. [PubMed: 18443335]

[8]. Parazzini F, Hum. Reprod 1999, 14, 1332. [PubMed: 10325288]

[9]. Marcoux S, Maheux R, Berube S, N. Engl. J. Med 1997, 337, 217. [PubMed: 9227926]

[10]. Tandoi I, Somigliana E, Riparini J, Ronzoni S, Vigano P, Candiani M, J. Pediatr. Adolesc .Gynecol 2011, 24, 376. [PubMed: 21906976]

[11]. Guo SW, Hum. Reprod. Update 2009, 15, 441. [PubMed: 19279046]

[12]. Kikuchi I, Takeuchi H, Kitade M, Shimanuki H, Kumakiri J, Kinoshita K, Acta Obstet. Gynecol. Scand 2006, 85, 1120. [PubMed: 16929419]

[13]. van Dam GM, Themelis G, Crane LM, Harlaar NJ, Pleijhuis RG, Kelder W, Sarantopoulos A, de Jong JS, Arts HJ, van der Zee AG, Bart J, Low PS, Ntziachristos V, Nat. Med 2011, 17, 1315. [PubMed: 21926976]

[14]. Hoogstins CE, Tummers QR, Gaarenstroom KN, de Kroon CD, Trimbos JB, Bosse T, Smit VT, Vuyk J, van de Velde CJ, Cohen AF, Low PS, Burggraaf J, Vahrmeijer AL, Clin. Cancer Res 2016, 22, 2929. [PubMed: 27306792]

[15]. Handgraaf HJ, Verbeek FP, Tummers QR, Boogerd LS, van de Velde CJ, Vahrmeijer AL, Gaarenstroom KN, Gynecol. Oncol 2014, 135, 606. [PubMed: 25124160]

[16]. Song J, Zhang L, Yi H, Huang J, Zhang N, Zhong Y, Hao L, Ke Y, Wang Z, Wang D, Yang Z, Nanomedicine 2019, 20, 102020. [PubMed: 31125675]

[17]. Krempien R, Roeder F, Radiat. Oncol 2017, 12, 8. [PubMed: 28069018]

[18]. Zilidis G, Aziz F, Telara S, Eljamel MS, Photodiagn. Photodyn. Ther 2008, 5, 264.

[19]. Anbil S, Rizvi I, Celli JP, Alagic N, Pogue BW, Hasan T, J. Biomed. Optics 2013, 18, 098004.

[20]. Triesscheijn M, Baas P, Schellens JH, Stewart FA, The Oncologist 2006, 11, 1034. [PubMed: 17030646]

[21]. Molpus KL, Kato D, Hamblin MR, Lilge L, Bamberg M, Hasan T, Cancer Res. 1996, 56, 1075. [PubMed: 8640764]

[22]. Kim JY, Choi WI, Kim M, Tae G, J. Controlled Release 2013, 171, 113.

[23]. Taratula O, Doddapaneni BS, Schumann C, Li X, Bracha S, Milovancev M, Alani A, Taratula O, Chem. Mater 2015, 27, 6155.

[24]. Duong T, Li X, Yang B, Schumann C, Albarqi HA, Taratula O, Taratula O, Nanomedicine 2017, 13, 955. [PubMed: 27884637]

[25]. Chen Y, Li L, Chen W, Chen H, Yin J, Chinese Chem. Lett 2019, 30, 1353.

[26]. Li Y, Lin TY, Luo Y, Liu Q, Xiao W, Guo W, Lac D, Zhang H, Feng C, Wachsmann-Hogiu S, Walton JH, Cherry SR, Rowland DJ, Kukis D, Pan C, Lam KS, Nature Commun. 2014, 5, 4712. [PubMed: 25158161]

[27]. Sheng Z, Hu D, Zheng M, Zhao P, Liu H, Gao D, Gong P, Gao G, Zhang P, Ma Y, Cai L, ACS Nano 2014, 8, 12310. [PubMed: 25454579]

[28]. Xiao YF, An FF, Chen JX, Yu J, Tao WW, Yu Z, Ting R, Lee CS, Zhang XH, Small 2019, 15, e1903121. [PubMed: 31379108]

[29]. Wei J-P, Chen X-L, Wang X-Y, Li J-C, Shi S-G, Liu G, Zheng N-F, Chinese Chem. Lett 2017, 28, 1290.

[30]. Taratula O, Schumann C, Duong T, Taylor KL, Taratula O, Nanoscale 2015, 7, 3888. [PubMed: 25422147]

[31]. Frangioni JV, Curr. Opin. Chem. Biol 2003, 7, 626. [PubMed: 14580568]

[32]. Schaafsma BE, Mieog JS, Hutteman M, van der Vorst JR, Kuppen PJ, Lowik CW, Frangioni JV, van de Velde CJ, Vahrmeijer AL, J. Surg. Oncol 2011, 104, 323. [PubMed: 21495033]

[33]. Gibbs SL, Quant. Imaging Med. Surg 2012, 2, 177. [PubMed: 23256079]

[34]. Li X, Schumann C, Albarqi HA, Lee CJ, Alani AWG, Bracha S, Milovancev M, Taratula O, Taratula O, Theranostics 2018, 8, 767. [PubMed: 29344305]

[35]. Slayden OD, Mah K, Brenner RM, Biol. Reprod. 1996, 54, 77.

[36]. Rotgeri A, Korolainen H, Sundholm O, Schmitz H, Fuhrmann U, Prelle K, Sacher F, Hum. Reprod 2015, 30, 308. [PubMed: 25432919]

[37]. Maeda H, Nakamura H, Fang J, Adv. Drug Delivery Rev 2013, 65, 71.

[38]. Zhang H, Li J, Sun W, Hu Y, Zhang G, Shen M, Shi X, PLoS One 2014, 9, e94718. [PubMed: 24722347]

[39]. Guo X, Li W, Zhou J, Hou W, Wen X, Zhang H, Kong F, Luo L, Li Q, Du Y, You J, Small 2017, 13.

[40]. Rocha AL, Reis FM, Taylor RN, Obstet. Gynecol. Int 2013, 2013, 859619. [PubMed: 23766765]

[41]. Cuong NV, Jiang JL, Li YL, Chen JR, Jwo SC, Hsieh MF, Cancers 2010, 3, 61. [PubMed: 24212606]

[42]. Aghajanova L, Giudice LC, Reprod. Sci 2011, 18, 229. [PubMed: 21063030]

[43]. Albarqi HA, Wong LH, Schumann C, Sabei FY, Korzun T, Li X, Hansen MN, Dhagat P, Moses AS, Taratula OR, Taratula O, ACS Nano 2019, 13, 6383. [PubMed: 31082199]

[44]. Dani RK, Schumann C, Taratula O, Taratula O, AAPS Pharm. Sci. Tech 2014, 15, 963.

[45]. Schumann C, Chan S, Khalimonchuk O, Khal S, Moskal V, Shah V, Alani AW, Taratula O, Taratula O, Mol. Pharmaceutics 2016, 13, 2070.

[46]. Schumann C, Taratula O, Khalimonchuk O, Palmer AL, Cronk M, Jones CV, Escalante CA, Taratula O, Nanomedicine 2015, 11, 1961. [PubMed: 26238076]

[47]. Taratula O, Savla R, Minko T, Int. J. Nanotechnol 2011, 8, 36.

[48]. Taratula O, Schumann C, Naleway MA, Pang AJ, Chon KJ, Taratula O, Mol. Pharmaceutics 2013, 10, 3946.

[49]. Haining REB, Cameron IT, van Papendorp C, Davenport AP, Prentice A, Thomas EJ, Smith SK, Hum. Reprod 1991, 6, 1200. [PubMed: 1752919]

[50]. Greenberg LH, Slayden OD, Am. J. Obstet. Gynecol 2004, 190, 1788. [PubMed: 15284801]

[51]. Sykes EA, Chen J, Zheng G, Chan WC, ACS Nano 2014, 8, 5696. [PubMed: 24821383]

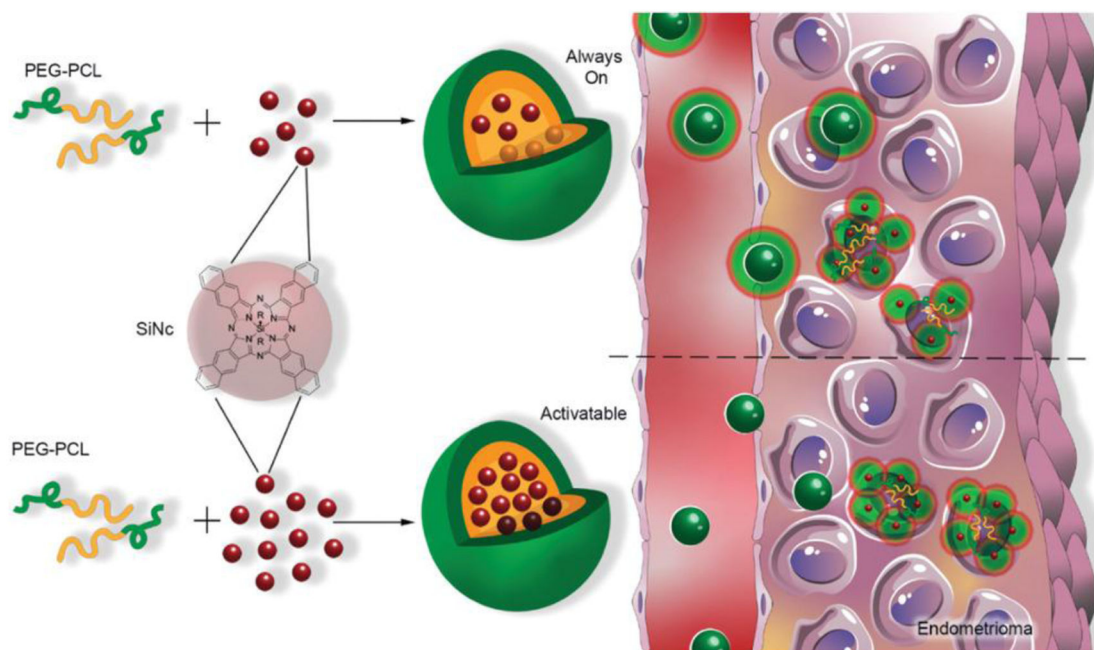**Figure 1.**
Schematic illustration of "always on" and "activatable" SiNc-loaded PEG-PCL
nanoparticles (SiNc-NP). Green and orange colors represent hydrophilic PEG outer shell
and hydrophobic PCL core of nanoparticles, respectively. In contrast to 'always on" SiNc-
NP (top panel), "activatable" SiNc-NP (lower panel) contain a higher amount of SiNc
molecules (dark red spheres) inside the hydrophobic cores, causing fluorescence self-
quenching. "Activatable" SiNc-NP generate fluorescence after internalization into
endometriotic cells and subsequent relaxation of densely-packed, self-quenched SiNc
molecules in the intracellular environment.
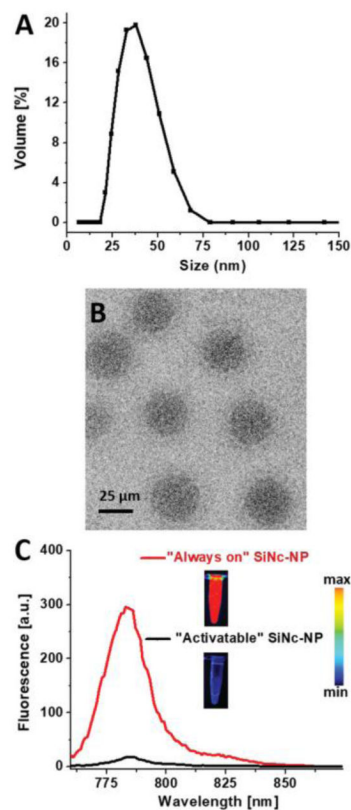
Figure 2.
A) Representative dynamic light scattering profile and B) cryo-TEM image of SiNc-loaded PEG-PCL nanoparticles (SiNc-NP). Scale bar is 25 μm in (B). C) Fluorescence spectra (excitation wavelength = 750 nm) of SiNc-NP with low (0.5% SiNc/1 mg PEG-PCL, "always on" SiNc-NP) and high (6% SiNc/1 mg PEG-PCL, "activatable" SiNc-NP) SiNc loading. Inset: fluorescence images of "always on" and "activatable" SiNc-NP solutions acquired using the Pearl Impulse Small Animal Imaging System. Scale bar: The blue and red colors reflect the lowest and highest fluorescence intensity, respectively.
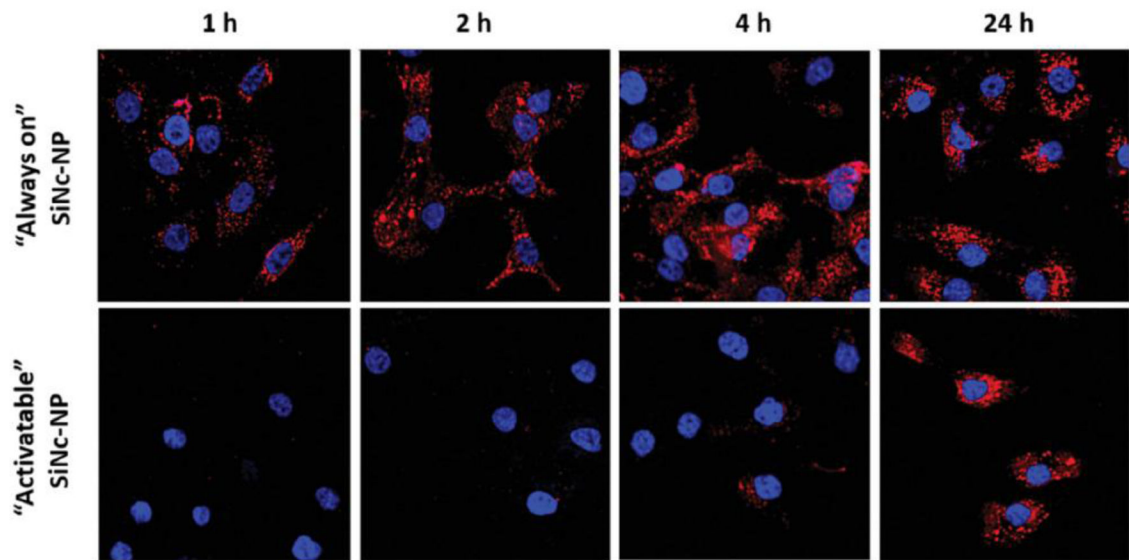
Figure 3.
Representative fluorescence microscopy images of macaque endometriotic stromal cells incubated with "always on" SiNc-NP (top panel) and "activatable" SiNc-NP (low panel) for 1, 2, 4, and 24 h. The red and blue colors reflect the fluorescence signal generated by SiNc and NucBlue (nuclei staining), respectively.
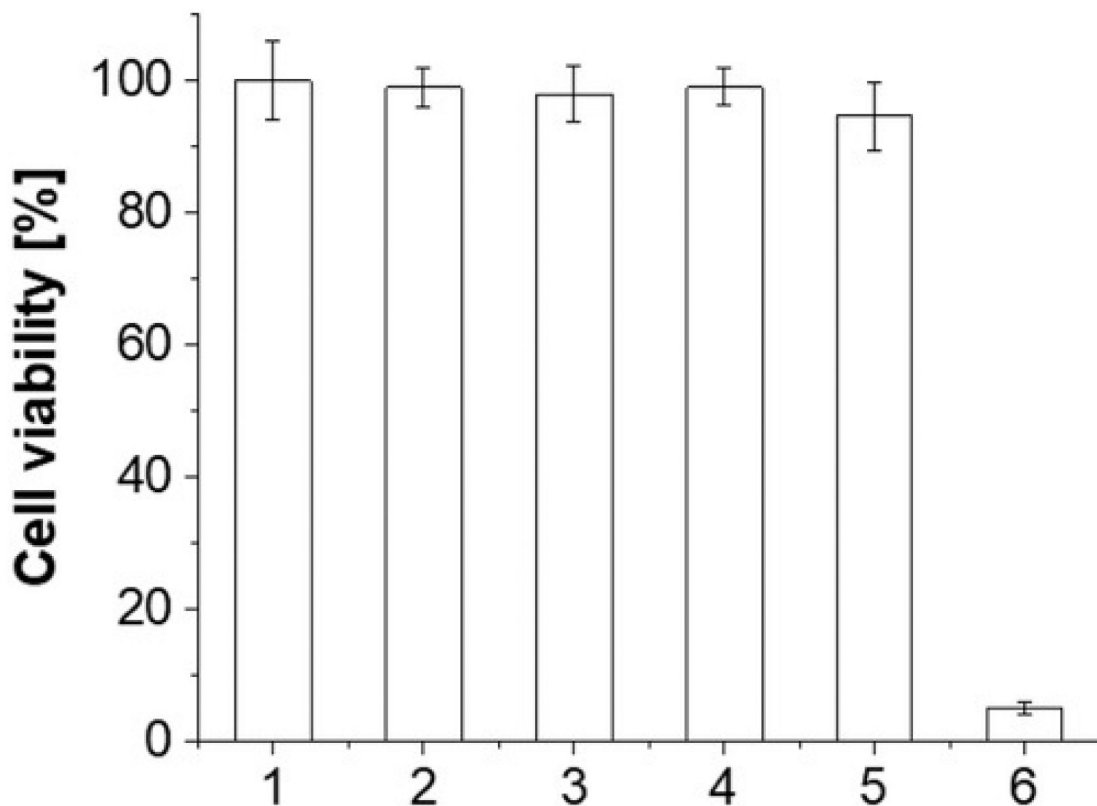
Figure 4.
Viability of macaque endometriotic stromal cells after the following treatments: 1) cells incubated with medium; 2) cells exposed to 780 nm NIR light ($0.9\ W\ cm^{-2}$) for 15 min; 3) cells incubated with empty PEG-PCL nanoparticles (without SiNc) for 48 h;4) cells incubated with empty PEG-PCL nanoparticles for 48 h and exposed to 780 nm NIR light ($0.9\ W\ cm^{-2}$) for 15 min; 5) cells incubated with "activatable" SiNc-NP ($SiNc=30\mu g\ mL^{-1}$) for 48 h; 6) cells incubated with "activatable" SiNc-NP ($SiNc = 30\ \mu g\ mL^{-1}$) for 48 h and exposed to 780 nm NIR light ($0.9\ W\ cm^{-2}$) for 15 min. $*p < 0.05$ when compared with the control (bar 1).
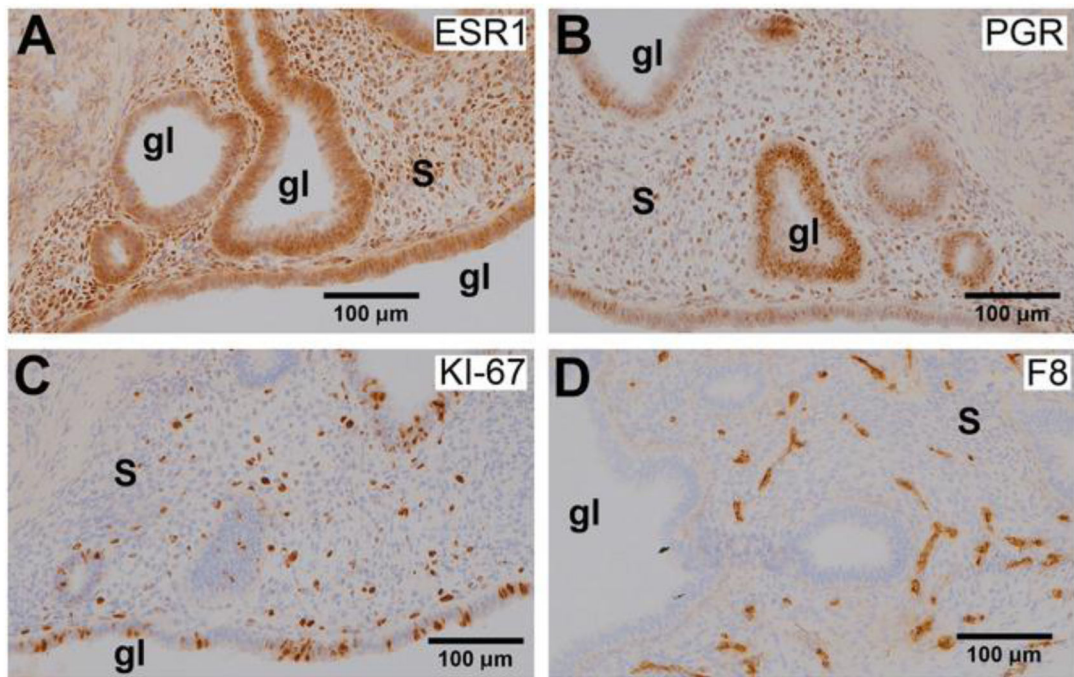
Figure 5.
Photomicrographs showing immunohistochemical staining (brown color) for A) ESR1, B) PGR, C) KI-67, and D) Factor 8 in endometriotic grafts collected from non-treated mice. All images captured at 20× magnification; "s" indicates stroma and "gl" indicates glands.
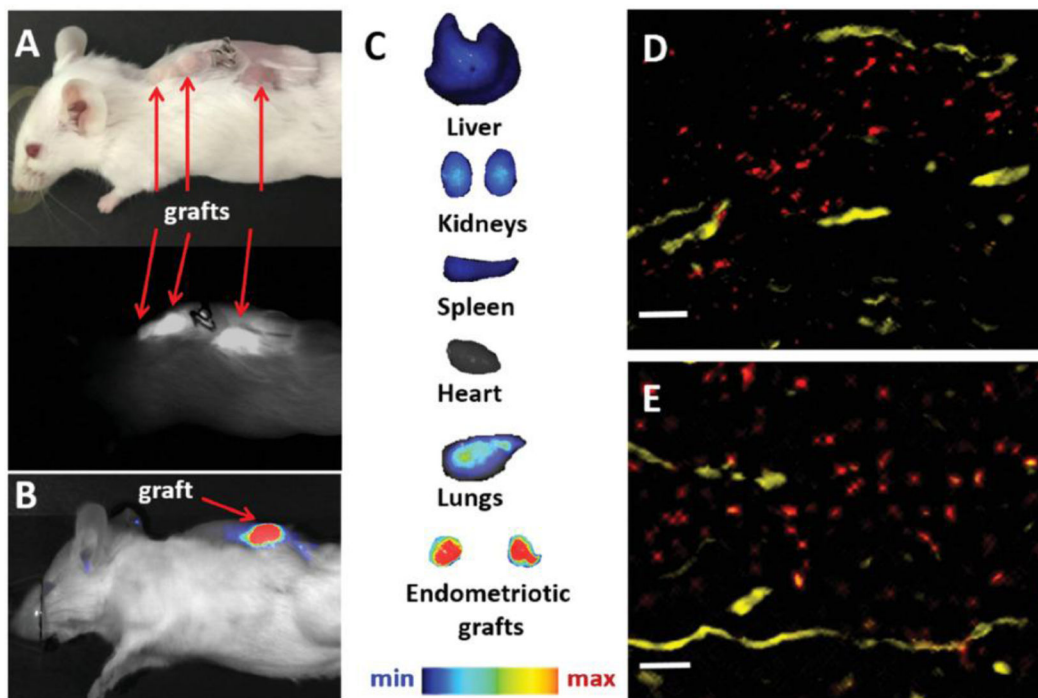
Figure 6.
A) Photograph (top) and NIR fluorescence image (bottom), recorded with Fluobeam 800, of a mouse bearing endometriotic grafts 24 h after intravenous injection of "activatable" SiNc-NP. B,C) NIR fluorescence images of a mouse bearing endometriotic graft (B) and resected tissues (C) recorded with Pearl Impulse Small Animal Imaging System 24 h after intravenous injection of "activatable" SiNc-NP. D,E) Representative fluorescence microscopy images of sections of endometriotic grafts collected 24 h after intravenous injection of SiNc-NP. Red color indicates NIR fluorescence generated by SiNc-NP. Yellow color represents blood vessels stained with the fluorescently labeled anti-CD31 antibody. Scale bars are 50 μm.
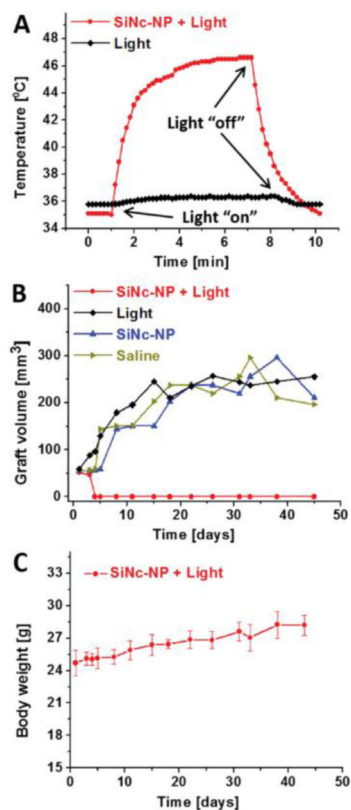
Figure 7.
A) Representative temperature profile inside of endometriotic graft during photothermal therapy (PTT) mediated by intravenously injected SiNc-NP in combination with 780 nm light (0.9 W cm^{-2}, red curve). Mice were injected with SiNc-NP 24 h prior to NIR light treatment. The black curve represents a temperature profile inside of endometriotic graft upon exposure to 780 nm light only (without SiNc-NP injection). B) Representative growth profiles of subcutaneous endometriotic grafts after the following treatments: 1) saline, mice injected with saline; 2) SiNc-NP, mice injected intravenously with SiNc-NP (3 mg SiNc kg^{-1}); 3) light, mice injected with saline and exposed to 780 nm light (0.9 W cm^{-2}) for 15 min at 24 h post-injection; 4) SiNc-NP + light, mice injected intravenously with SiNc-NP (3 mg SiNc kg^{-1}) and exposed to 780 nm light (0.9 W cm^{-2}) for 15 min at 24 h post-injection. C) Changes in body weights of mice injected intravenously with SiNc-NP (3 mg SiNc kg^{-1}) and exposed to 780 nm light for 15 min at 24 h post-injection.
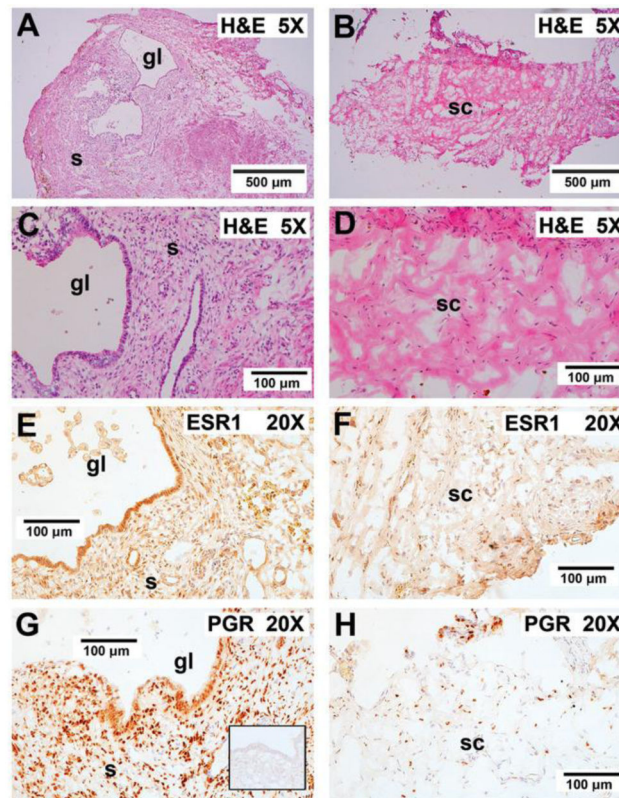
Figure 8.
Effect of PTT on graft histology and steroid receptor staining. A,C) In control mice not receiving PTT, the grafts displayed enlarged endometriotic glands and stroma. E,G) In these mice, the grafts stained strongly for both ESR1 and PGR. B,D) Endometriotic glands and stroma were lost after PTT and graft sites were replaced with murine connective tissue. F,H) Minimal ESR1 and PGR staining nuclei were observed after PTT therapy. The inset in G shows irrelevant IgG control (anti-Br(d) U) showing staining specificity for both ESR1 and PGR. "gl" indicates glands; "s" indicates stroma; "sc" indicates stromal connective tissue with minimal ESR1 and PGR staining. 5X, 5× plan apochromatic objective; 20X, 20× plan apchromatic objective.